International Journal of Solids and Structures 47 (2010) 3034–3049

Contents lists available at ScienceDirect

International Journal of Solids and Structures

journal homepage: www.elsevier.com/locate/ijsolstr

Contact analysis in presence of spherical inhomogeneities within a half-space

J. Leroux, B. Fulleringer, D. Nélias *

Université de Lyon, CNRS INSA-Lyon, LaMCoS UMR5259, F-69621, France

ARTICLE INFO

Article history:
Received 23 March 2010
Received in revised form 14 June 2010
Available online 16 July 2010

Keywords:
Inhomogeneity
Inclusion
Contact mechanics

ABSTRACT

This paper presents a fast method of solving contact problems when one of the mating bodies contains multiple heterogeneous inclusions, and numerical results are presented for soft or stiff inhomogeneities. The emphasis is put on the effects of spherical inclusions on the contact pressure distribution and subsurface stress field in an elastic half-space. The computing time and allocated memory are kept small, compared to the finite element method, by the use of analytical solution to account for the presence of inhomogeneities. Eshelby's equivalent inclusion method is considered in the contact solver. An iterative process is implemented to determine the displacements and stress fields caused by the eigenstrains of all spherical inclusions. The proposed method can be seen as an enrichment technique for which the effect of heterogeneous inclusions is superimposed on the homogeneous solution in the contact algorithm. 3D and 2D Fast Fourier Transforms are utilized to improve the computational efficiency. Configurations such as stringer and cluster of spherical inclusions are analyzed. The effects of Young's modulus, Poisson's ratio, size and location of the inhomogeneities are also investigated. Numerical results show that the presence of inclusions in the vicinity of the contact surface could significantly changes the contact pressure distribution. From a numerical point of view the role of Poisson's ratio is found very important. One of the findings is that a relatively 'soft' and nearly incompressible inclusion – for example a cavity filled with a liquid – can be more detrimental for the stress state within the matrix than a very hard inclusion with a classical Poisson's ratio of 0.3.

1. Introduction

The presence of voids or inclusions creates incompatibility of deformations between the inclusions and the surrounding matrix, which creates initial stresses and modifies the stress field during loading. It is well known that, for a contact problem, hard inclusions act as stress raisers and damage initiation sites (Voskamp, 1985; Nélias et al., 1999), reducing the service life of the component. Usually this problem is treated numerically. However most of the time the contact problem is not solved explicitly and a Hertzian pressure distribution is assumed (Kabo and Ekberg, 2002, 2005; Courbon et al., 2005) instead.

The problem of the inclusion in an infinite matrix has been investigated by many (hundreds of) researchers following the pioneering work of Edward (1951), Eshelby (1957, 1959, 1961), Willis (1964), Walpole (1967), Asaro and Barnett (1975) and Mura and Furuhashi (1984). Early work by Eshelby (1957, 1959, 1961) initiated a versatile and powerful method dealing with the perturbation of an uniform field by an ellipsoidal inhomogeneity, and shows that an ellipsoidal heterogeneous inclusion with uniform eigenstrain induces a constant stress state within the inclusion. In the terminology of Eshelby, an 'inclusion' is a region in an elastic medium which has the same elastic properties as the matrix, but which is subjected to either elastic or inelastic strains, also called 'eigenstrains'. On the other hand, an inhomogeneity is a region with properties distinct from those of the surrounding material and subjected to an applied stress. Hence, a 'heterogeneous inclusion' also simply denoted 'inclusion' could be referred to as 'inhomogeneity' in the sense of Eshelby.

A high number of inclusion problems has been solved since the pioneering work of Eshelby, as pointed out by the extensive reviews of Mura (1987, 1988). The elastic solution for an inclusion with uniform eigenstrains near the free surface of a semi-infinite solid has been obtained for a spherical inclusion with hydrostatic eigenstrain (Mindlin and Cheng, 1950), a spherical inclusion with arbitrary eigenstrains (Aderogba, 1976), a cuboidal inclusion with incompressible eigenstrains (Chiu, 1977, 1978), and an ellipsoidal inclusion with pure dilatational eigenstrain (Seo and Mura, 1970).

However, many results at present are not expressed explicitly but are obtained numerically. Miller and Keer (1993) presented a two-dimensional contact stress analysis with a rigid indenter sliding with friction on a half-space containing a near-surface circular inclusion. This problem is analyzed numerically by using complex variable formulation of Muskhelishivii. Kuo (2007, 2008) studied the effects of multiple spherical or ellipsoidal inclusions on the

* Corresponding author. Tel.: +33 4 72 43 84 90; fax: +33 4 72 43 89 13.
E-mail address: daniel.nelias@insa-lyon.fr (D. Nélias).

0020-7683/$ - see front matter © 2010 Elsevier Ltd. All rights reserved.
doi:10.1016/j.ijsolstr.2010.07.006

Nomenclature

Letters

a	contact radius for contact problem
a or r	inclusion radius
B_{ijkl}	influence coefficients that relate the stress σ_{ij} at point (x_1,x_2,x_3) to the constant eigenstrain at the point (x_1^k,x_2^k,x_3^k)
C^m_{ijkl}, C^i_{ijkl}	elastic constants of the matrix and the inhomogeneity
D_{ijkl}, D_{ijklm}	coefficients of E^*_{ij}, E^*_{ijk}, etc. in the strain field due to the eigenstrain
e_{ij}	uniform dilatation eigenstrains
E_m, E_i	Young's modulus of the matrix m and the inhomogeneity i
E^*_{ijk}	terms in the decomposition of the eigenstrain ε^*_{ij} in Taylor series
K^n	coefficients in the normal displacement at the contact surface due to contact pressure
M_{ij}	influence coefficients that relate the stress σ_{ij} at point (x_1,x_2,x_3) to the normal traction σ^n within a discretized area centered at $(x_1^k,x_2^k,0)$
n_1, n_2, n_3	grid number in the half-space along the Cartesian directions x_1, x_2, x_3, respectively
P	contact pressure distribution
P_0	maximum Hertzian pressure
R	indenter radius
S_{ijkl}	components of the Eshelby's tensor
T	temperature
$x^I=(x_1^I,x_2^I,x_3^I)$	Cartesian coordinates of the inclusion center
$x^k=(x_1^k,x_2^k,x_3^k)$	Cartesian coordinates of kth inclusion center

Greek letters

ε^∞_{ij}	infinite applied strain
ε^*_{ij}	eigenstrain due to the presence of inhomogeneties
ε_{ij}	strain due to eigenstrain ε^*_{ij}
σ_{ij}	total stress due to eigenstrains
ϕ, ψ	harmonic and biharmonic potentials of mass density ε^*_{ij}
$\phi_{ij\ldots}$, $\psi_{ij\ldots}$	harmonic and biharmonic potentials of mass density $x_ix_j\ldots$
δ_{ij}	Kronecker symbol
Ω_i	ith inclusion domain
ε^k_{ij}	strain due to eigenstrain ε^*_{ij} of the kth inclusion
σ_n	normal pressure due to the summation of both symmetric inclusions
Δx_1, Δx_2	half size of discretized surface area
α	thermal expansion coefficient
ν	Poisson's ratio of the half-space
ν_m, ν_i	Poisson's ratio of the matrix m and the inhomogeneity i
γ	Young's modulus ratio
τ_m	maximum shear stress

Acronyms and fast Fourier transforms

2D-FFT	two-dimensional fast Fourier transform
3D-FFT	three-dimensional fast Fourier transform
FFT^{-1}	inverse FFT operation
$\widehat{B}_{ijkl}$	frequency response of coefficients B_{ijkl} in the frequency domain
$\widehat{M}_{ij}$	frequency response of coefficients M_{ij} in the frequency domain

contact pressure and subsurface stresses in an elastic half-space. This two-dimensional contact stress analysis used a boundary element method, where the results are obtained by solving a set of integral equations numerically.

Chiu (1977, 1978) has solved the stress field due to uniform eigenstrains in a cuboidal inclusion surrounded by an infinite elastic space and a half-space, respectively, but most of the works by other authors have been done for ellipsoidal inclusions.

The purpose of this paper is to propose a comprehensive method for solving contact problems in the presence of subsurface inhomogeneities such as voids or cavities, inclusions, or fibbers. The proposed method is based on the use of fully analytical solutions available in the literature for simple shapes (sphere, cylinder, cuboid, etc.). However, it should be noted that the procedure could be easily extended to more complicated or general geometries without additional difficulty, except that it will require the determination of the Green's function numerically. It should be noted that the procedure could be easily extended to more complicated or general geometries without additional difficulty, except that it will require the determination of the Green's function numerically. It should also be mentioned that the principle of this method, which was previously and successfully employed for elasto-plastic contact problems with a plastic zone discretized into small cuboids (Jacq et al., 2002), is very close to the enrichment techniques. The enrichment technique, used elsewhere for example in the Extended Finite Element Method (X-FEM), consists of superimposing a numerical or analytical field at some points of a mesh into a numerical scheme, independently of the initial mesh. The capabilities of the proposed technique are illustrated here by the analysis of the effects of multiple heterogeneous and spherical inclusions on the contact pressure distribution and subsurface stress field for a frictionless circular point contact.

It is worth noting that the distribution of the Hertz contact pressure may be affected by the presence of inclusions near the contact surface. When multiple inclusions exist and interact within the material, the strain and stress fields become even more complicated. Furthermore, the constrained strain in an inhomogeneity is non uniform due to the presence of the contact interface. Moschovidis and Mura (1975) and Mura (1987) described a method that uses a quadratic development of the strain field around the centre of each inclusion. However, the applied strain will be treated as uniform in this paper. To investigate the effects of interacting inhomogeneities with uniform eigenstrains on the strain field, a three-dimensional contact analysis is presented for a spherical tip indenting an elastic half-space containing multiple inhomogeneities.

2. Equivalent inclusion method

In the earliest formulation of Eshelby the strain field at infinity (or the strain field in the matrix without the heterogeneous inclusion) is uniform. For a contact problem where strong gradients are present it usually means that the size of the inhomogeneity is small compared to the contact dimensions. For inhomogeneity of larger size it is, however, possible to discretize it in several smaller elements so that the size of each of them remains small in comparison to the contact dimensions. For the notation in what follows, subscripts (i,j,k,l) range over 1, 2, 3, and the index summation convention holds.

2.1. Eshelby solution

A matrix D having stiffness tensor C^M_{ijkl} is submitted to a uniform applied strain ε^∞_{ij}. The stress σ_{ij} is obtained by the Hooke's law due to the hypothesis of linear isotropic elasticity:

$$\sigma_{ij}^{\infty} = C_{ijkl}^{M}\varepsilon_{kl}^{\infty}. \tag{1}$$

The presence of a heterogeneous inclusion of stiffness tensor $C_{ijkl}^{I} \neq C_{ijkl}^{M}$ induces a strain ε_{ij}. The stress σ_{ij} is related by:

$$\text{In the inclusion } \Omega, \qquad \sigma_{ijkl} = C_{ijkl}^{I}\left(\varepsilon_{kl}^{\infty} + \varepsilon_{kl}\right), \tag{2}$$

$$\text{In the matrix } D, \qquad \sigma_{ijkl} = C_{ijkl}^{M}\left(\varepsilon_{kl}^{\infty} + \varepsilon_{kl}\right). \tag{3}$$

According to Eshelby, an ellipsoidal inhomogeneity can be replaced by an equivalent inclusion which has the same elastic properties C_{ijkl}^{M}, but which is subject to an additional imaginary strain or 'eigenstrain' ε_{ij}^{*} such that:

$$\sigma_{ij} = C_{ijkl}^{I}\left(\varepsilon_{kl}^{\infty} + \varepsilon_{kl}\right) = C_{ijkl}^{M}\left(\varepsilon_{kl}^{\infty} + \varepsilon_{kl} - \varepsilon_{kl}^{*}\right), \quad \text{in } \Omega. \tag{4}$$

Eq. (4) is necessary and sufficient for equivalency of the inhomogeneity and the inclusion problems. The "equivalent inclusion" method requires to determine the eigenstrain ε_{ij}^{*} which is related to compatibility strain ε_{ij} by:

$$\varepsilon_{ij} = S_{ijkl} \times \varepsilon_{kl}^{*}, \tag{5}$$

where S_{ijkl} is the Eshelby's tensor which will be discussed in greater details in Section 2.2.

Thus Eqs. (4) and (5) allow us to determine the strain ε_{ij}^{*} and ε_{ij} inside the inclusion. Mura (1987) describes the expression of the Green's functions that allow to calculate ε_{ij} and σ_{ij} outside the inclusion in a half-space.

2.2. Determination of compatibility strain

There is no general analytical solution when several inhomogeneities are randomly distributed in an infinite matrix. The Eshelby solution (Eshelby, 1957, 1959) is an exact one for a single ellipsoidal inclusion in an infinite matrix. However it is possible to study the effect of each of them and then superimpose the solutions. Moschovidis and Mura (1975) proposed to develop the eigenstrain ε_{ij}^{*} as a Taylor series:

$$\varepsilon_{ij}^{*}(x) = E_{ij}^{*} + E_{ijk}^{*}x_k + E_{ijkl}^{*} \cdot x_k \cdot x_l + \cdots \tag{6}$$

The compatibility strain ε_{ij} now emerges from a complex function $D_{ijkl}(x)$:

$$\varepsilon_{ij}(x) = D_{ijkl}(x)E_{kl}^{*} + D_{ijklq}(x)E_{klq}^{*} + D_{ijklqr}(x)E_{klqr}^{*} + \cdots \tag{7}$$

The function $D_{ijkl}(x)$ is derived from harmonic $\phi_{ij}(x)$ and biharmonic $\psi_{ij}(x)$ potentials defined as follow:

$$\begin{aligned}
\psi(x) &= \int\int_{\Omega}\int |x - x'|dx', \\
\psi_{ij\ldots k}(x) &= \int\int_{\Omega}\int x_i'x_j'\ldots x_k'|x - x'|dx', \\
\phi(x) &= \int\int_{\Omega}\int \frac{dx'}{|x - x'|}, \\
\phi_{ij\ldots k}(x) &= \int\int_{\Omega}\int \frac{x_i'x_j'\ldots x_k'dx'}{|x - x'|}.
\end{aligned} \tag{8}$$

In the current instance, only the first term of Eq. (7) is considered:

$$\varepsilon_{ij}(x) = D_{ijkl}(x)E_{kl}^{*}, \quad \text{in the matrix } D, \tag{9}$$

where

$$\begin{aligned}
D_{ijkl}(x) = {} & \frac{1}{8\pi(1-\nu)}\left[\psi(x)_{,klij} - 2\nu\delta_{kl}\phi(x)_{,ij}\right] \\
& - \frac{1}{8\pi}\left[\phi(x)_{,kj}\delta_{il} + \phi(x)_{,ki}\delta_{jl} + \phi(x)_{,lj}\delta_{ik} + \phi(x)_{,li}\delta_{jk}\right].
\end{aligned} \tag{10}$$

The above manipulation becomes of practical interest for the case when the domain Ω is an ellipsoid with principal axes lying along the axes x_1, x_2, x_3 of the coordinate system, and particularly for a spherical inhomogeneity. In this case the potentials given by Eq. (8) can be calculated explicitly and analytically. It is noted that the eigenstrain is uniform for a spherical inclusion of radius a and center $x^I = (x_1^I, x_2^I, x_3^I)$ with an uniform applied strain $\varepsilon_{ij}^{\infty}$.

$$\text{In the inclusion } \Omega: \quad \begin{aligned} \phi &= \tfrac{4}{3}\pi a^2\left(\tfrac{3}{2} - \tfrac{1}{2}\tfrac{r^2}{a^2}\right), \\ \psi &= \tfrac{4}{3}\pi a^4\left(\tfrac{3}{4} + \tfrac{1}{2}\tfrac{r^2}{a^2} - \tfrac{1}{20}\tfrac{r^4}{a^4}\right), \end{aligned} \tag{11}$$

$$\text{In the matrix } D: \quad \begin{aligned} \phi &= \tfrac{4}{3}\pi a^2\tfrac{a}{r}, \\ \psi &= \tfrac{4}{3}\pi a^4\left(\tfrac{1}{5}\tfrac{a}{r} + \tfrac{r}{a}\right), \end{aligned} \tag{12}$$

where

$$r = \sqrt{\left(x_1 - x_1^I\right)^2 + \left(x_2 - x_2^I\right)^2 + \left(x_3 - x_3^I\right)^2}. \tag{13}$$

The Eshelby's tensor S_{ijkl} is obtained from Eqs. (10) and (11) such that:

$$S_{ijkl} = D_{ijkl}(x^I). \tag{14}$$

Thus, the Moschovidis solution (Moschovidis and Mura, 1975) permits determination of ε_{ij} and σ_{ij} inside and outside the inhomogeneity. The above procedure can be easily generalized for more than one inhomogeneity. Let n inhomogeneities, designed by subscripts $1, 2, \ldots, n$, be present in the matrix occupying the domains $\Omega_1, \Omega_2, \ldots, \Omega_n$. The presence of the inhomogeneities induces a self-equilibrated elastic field characterized by $\varepsilon_{ij}(x)$, such that the total elastic field due to the applied field and the inhomogeneities is $\varepsilon_{ij}^{\infty}(x) + \varepsilon_{ij}(x)$.

The "equivalent inclusion" method requires to determine the eigenstrains for each inclusion, defined in their respective domain, from the condition that the induced strain field by these eigenstrains should be the same as the one induced by the inhomogeneities. The above condition is expressed by the equivalency equations that the eigenstrains have to satisfy identically for every point x. Assuming that the deformation is small and within the limit of linear elasticity theory, the compatibility strain ε_{ij} results from the sum of the contributions of each inclusion k at the point x:

$$\varepsilon_{ij}(x) = \sum_{k=1}^{n}\varepsilon_{ij}^{k}(x). \tag{15}$$

2.3. Half-space solution

The three-dimensional contact problem involves to use a half-space which is bounded by the surface plane $x_3 = 0$ in the Cartesian coordinate system (x_1, x_2, x_3). It is then necessary to extend previous solutions, valid only for infinite spaces, to infinite half-spaces. Zhou et al. (2009) introduced a fast method for solving the problem of three-dimensional arbitrarily shaped inclusions in an isotropic half-space. The solution can be obtained by decomposing the problem into three subproblems and utilizing the solution for a spherical inclusion with uniform eigenstrain determined in an isotropic half-space.

(1) An inclusion with an eigenstrain $\underline{\varepsilon}^{*} = (\varepsilon_{11}^{*}, \varepsilon_{22}^{*}, \varepsilon_{33}^{*}, \varepsilon_{12}^{*}, \varepsilon_{13}^{*}, \varepsilon_{23}^{*})$ in an infinite space.
(2) A symmetric inclusion with an eigenstrain $\underline{\varepsilon}_{s}^{*} = (\varepsilon_{11}^{*}, \varepsilon_{22}^{*}, \varepsilon_{33}^{*}, \varepsilon_{12}^{*}, -\varepsilon_{13}^{*}, -\varepsilon_{23}^{*})$ in the same space.
(3) A normal traction distribution $-\sigma^{n}$ at the surface of the half-space ($x_3 = 0$) which is a function of eigenstrains ε^{*} and ε_{s}^{*}.

The stress field due to uniform eigenstrain within a spherical inclusion surrounded by an infinite elastic space has been given in an integral form by Mura (1987). The summation of the two solutions (1) and (2) generates only normal traction σ^{n} with no

tangential traction on $x_3 = 0$. Adding an opposite normal stress $-\sigma^n$ at the surface of the half-space leads to the creation of a free surface. This pressure field comes from the solution of σ_{33} induced by both inclusions.

The same approach will be used with many inhomogeneities. The solution for multiple inhomogeneities into a domain meshed with $n_1 \times n_2 \times n_3$ cuboids can be obtained by summing up the contribution of the eigenstrain produced by each inhomogeneity:

$$\begin{aligned}\sigma_{ij}(x_1,x_2,x_3) = &\sum_{x_3=0}^{n_3-1}\sum_{x_2=0}^{n_2-1}\sum_{x_1=0}^{n_1-1} B_{ijkl}(x_1-x_1^k,x_2-x_2^k,x_3-x_3^k)\,\varepsilon^*_{kl}(x_1^k,x_2^k,x_3^k)\\ &+\sum_{x_3=0}^{n_3-1}\sum_{x_2=0}^{n_2-1}\sum_{x_1=0}^{n_1-1} B_{ijkl}(x_1-x_1^k,x_2-x_2^k,x_3+x_3^k)\,\varepsilon^*_{s_{kl}}(x_1^k,x_2^k,-x_3^k)\\ &-\sum_{x_2=0}^{n_2-1}\sum_{x_1=0}^{n_1-1} M_{ij}(x_1-x_1^k,x_2-x_2^k,x_3)\,\sigma^n(x_1^k,x_2^k,0).\end{aligned} \tag{16}$$

B_{ijkl} are the influence coefficients that relate the stress σ_{ij} at point (x_1,x_2,x_3) to the constant eigenstrain at the point (x_1^k,x_2^k,x_3^k) which is the inclusion center in an infinite space

$$B_{ijkl}(x) = C^m_{ijmn}D_{mnkl}(x) \quad \text{for } x \text{ in } D-\Omega, \tag{17}$$

$$B_{ijkl}(x) = C^m_{ijmn}(D_{mnkl}(x)-1) \quad \text{for } x \text{ in } \Omega. \tag{18}$$

For a single inclusion centered at (x_1^k,x_2^k,x_3^k) in the half-space the normal traction σ^n at a surface point $(x'_1,x'_2,0)$ is obtained by:

$$\begin{aligned}\sigma_n(x'_1,x'_2) = &-B_{33kl}(x'_1-x_1^k,x'_2-x_2^k,-x_3^k)\,\varepsilon^*_{kl}(x_1^k,x_2^k,x_3^k)\\ &-B_{33kl}(x'_1-x_1^k,x'_2-x_2^k,x_3^k)\,\varepsilon^*_{s_{kl}}(x_1^k,x_2^k,x_3^k).\end{aligned} \tag{19}$$

M_{ij} represent the influence coefficients that relate the stress σ_{ij} at point (x_1,x_2,x_3) to the normal traction σ^n within a discretized area centered at $(x_1^k,x_2^k,0)$. In Eq. (16), each component $M_{ij}()$ is obtained by double integration of function $F_{ij}()$ over a discretized surface area $2\Delta x_1 \times 2\Delta x_2$ centered at $(x_1^k,x_2^k,0)$, see Appendices A and B

$$M_{ij}(x_1-x_1^k,x_2-x_2^k,x_3) = \int_{x_1^k-\Delta x_1}^{x_1^k+\Delta x_1}\int_{x_2^k-\Delta x_2}^{x_2^k+\Delta x_2} F_{ij}(x_1-x'_1,x_2-x'_2,x_3)\,dx'_1\,dx'_2. \tag{20}$$

One of problems encountered by Mura is the integration of this third term while σ^n is a complex function related to the influence of both inclusions on the stress σ_{33} at the contact surface. Thus it was easier to solve this integral with a particular case considering hydrostatic eigenstrains. The influence of the pressure field σ^n on stresses can be quantified using influence coefficient F_{ij} of pressure on stresses with numerical methods such as 2D-FFT. This method constitutes a semi-analytical approach removing the restrictions on the eigenstrains. The solution depends on the estimation of the normal traction σ^n which is most likely accurate on the contact domain. The surface is extended in order to get a good accuracy on the stress field in the volume.

The first and second summation terms in Eq. (16) are obtained by a 3D discrete convolution and the third term by a 2D discrete convolution in order to transform a triple summation into a simple summation of convolution products. It is noted that a combination of 3D and 2D-FFT algorithms can greatly reduce the computing time and the storage space (Zhou et al., 2009). Hence this numerical computation method can be performed on a fine mesh

$$\begin{aligned}\sigma_{ij}(x_1,x_2,x_3) = &FFT^{-1}\left(\widehat{B_{ijkl}}(x_1-x_1^k,x_2-x_2^k,x_3-x_3^k)\,\widehat{\varepsilon^*_{kl}}(x_1^k,x_2^k,x_3^k)\right)\\ &+FFT^{-1}\left(\widehat{B_{ijkl}}(x_1-x_1^k,x_2-x_2^k,x_3+x_3^k)\,\widehat{\varepsilon^*_{kl}}(x_1^k,x_2^k,-x_3^k)\right)\\ &-FFT^{-1}\left(\widehat{M_{ij}}(x_1-x_1^k,x_2-x_2^k,x_3)\,\widehat{\sigma^n}(x_1^k,x_2^k,0)\right).\end{aligned} \tag{21}$$

2.4. Normal displacement of a point at the surface

Inserting the equivalent eigenstrain into the total strain, the surface normal "eigen-displacement" can be calculated. Normal displacements are produced by the pressure field σ^n, while tangential displacements are produced by both inclusions and the pressure field. Only the normal displacements are obtained in this work by:

$$u_3(x_1,x_2) = \sum_{x'_2=0}^{n_2-1}\sum_{x'_1=0}^{n_1-1} K^n(x_1-x'_1,x_2-x'_2)\,\sigma_n(x'_1,x'_2). \tag{22}$$

The surface of interest is discretized into $n_1 \times n_2$ rectangular elements, each of which has a size of $2\Delta x_1 \times 2\Delta x_2$. Pressure and displacement of each discrete patch are treated as constant and their values are given at the patch center. The effect of an uniform pressure acting on a rectangular area has been analyzed in detail by Love (1927) and Johnson (1985). K^n are the influence coefficients that relate the normal displacement at the surface point $(x_1,x_2,0)$ to the normal pressure σ^n at the surface point $(x'_1,x'_2,0)$, see Appendix C.

The surface contact geometry is modified by adding the eigen-displacement and the contact pressure and shears are updated. The elastic displacements are calculated from the updated contact pressure. Therefore, this algorithm is repeated until convergence is obtained. A close-loop links the variations of the surface geometry, contact pressure and total strain, and is repeated until the difference between the eigen-displacements of two following iterative steps is less than the prescribed error. The flowchart of the inclusion part is shown in Fig. 1.

Note that for dissimilar elastic materials in frictional contact the tangential displacements of the surface points, given elsewhere in an analytical form by Fulleringer and Nélias (2010) for a cuboid of uniform eigenstrain, should not be neglected any more.

2.5. Contact solver

The core of the contact solver is based on the pioneering work of Jacq et al. (2002) who first introduced the effect of inelastic strains in a 3D contact algorithm based on semi-analytical methods. The algorithm was first applied to analyze an elastic–plastic contact (Jacq et al., 2002; Sainsot et al., 2002) and later a thermal-elastic–plastic contact (Boucly et al., 2005). Compared to the widely used finite element method (FEM) this numerical technique has two main advantages: first robustness and second low memory space required combined with an efficient numerical procedure that allows to solve transient 3D problem in less time than for a 2D problem by FEM. The contact solver may be also coupled with FEM to account for the flexibility of the structure and used as a structural zoom when a finer mesh is needed for the contact (Gallego et al., 2010). The method has since been developed and improved in several ways by the group of Nélias at INSA-Lyon (Nélias et al., 2006, 2007; Gallego et al., 2006, 2010; Gallego and Nélias, 2007; Antaluca and Nélias, 2008) and the group of Wang and Keer at Northwestern University (Liu and Wang, 2005; Liu et al., 2007; Chen et al., 2008a,b, 2007; Chen and Wang, 2008, 2009; Chen et al., 2009; Wang et al., 2009) to account for various plasticity models and tangential effects including running-in and

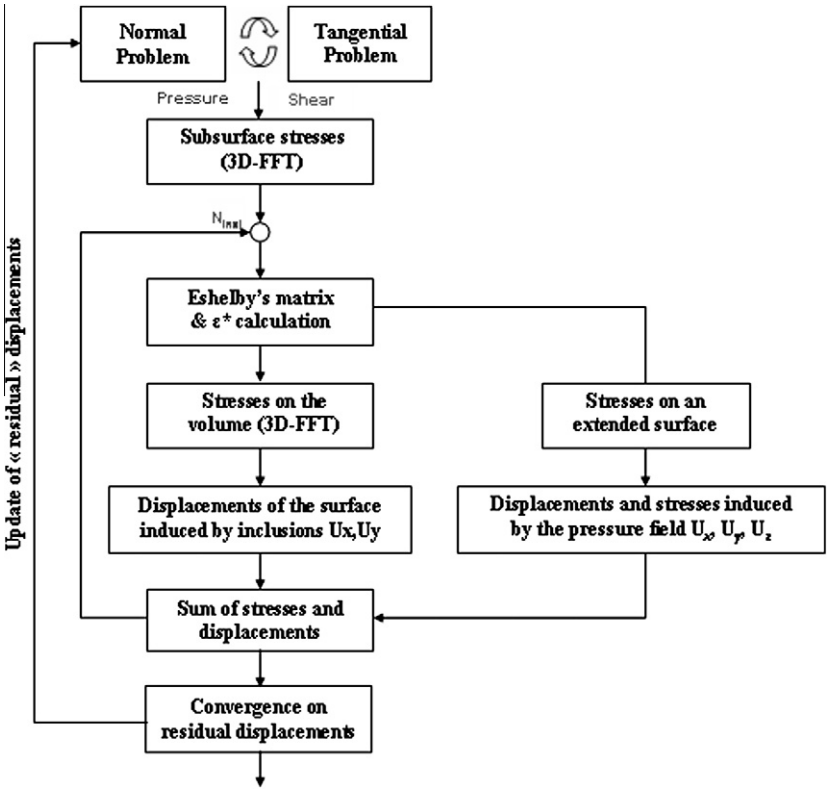

Fig. 1. Flowchart of the numerical procedure for the contact between heterogeneous bodies.

fretting wear. One interesting improvement is due to Zhou et al. (2009) who utilized a combination of three-dimensional and two-dimensional fast Fourier transform algorithms to decrease both the memory space allocated and the computing time. This improvement of the numerical procedure allows a finer discretization and a larger number of computation steps to be used.

2.6. Model validation

Mindlin and Cheng (1950) have found analytically the thermoelastic field due to a homogeneous sphere by using the method of potentials (MacMillan, 1930). Let Ω be a sphere of radius $a = 0.5c$ with center at $(0,0,c)$ in a half-space. The thermoelastic strain is expressed as $e_{ij} = \alpha T \delta_{ij}$ where α and T are the thermal expansion coefficient and temperature, respectively; δ is the Kronecker symbol i.e. $\delta_{ij} = 1$ when $i = j$ and $\delta_{ij} = 0$ otherwise. The inclusion is assumed to have uniform dilatation eigenstrain e_{ij}.

A comparison between the analytical solution of Mindlin and Cheng (1950) and the present numerical solution for a spherical inclusion with uniform dilatation eigenstrain is given in Fig. 2. Stresses are normalized by $\sigma_0 = E\alpha T/3(1-\nu)$. A very good agreement is found which in turn validates the numerical model and proves the efficiency of the proposed method. In Fig. 2(a), the component σ_{xx} is found continuous across the interface inclusion/matrix, satisfying the stress continuity condition at the interface. Conversely the two other components σ_{yy} and σ_{zz} are found discontinuous across the interface. In Fig. 2(b), the component σ_{zz} is continuous across the interface. The two other components σ_{xx} and σ_{yy} are identical and discontinuous across the interface.

3. Application to the frictionless indentation of an elastic half-space containing multiple heterogeneous inclusions

The method may be applied to nano-indentation, as schematically shown in Fig. 3. In this section, the Young's modulus and Poisson's ratio of the matrix are chosen as $E_m = 210$ GPa and $\nu_m = 0.3$, respectively. The indenter is rigid with a radius R of 105 μm. The maximum load P is 650 mN. For the homogeneous half-space, this load leads to a contact radius $a = 6.05$ μm and a maximum contact pressure $P_0 = 8469$ MPa. Note that in what follows the parameter a denotes now the contact radius and r the inclusion radius (in the previous section w/o contact problem a denoted the inclusion radius as in Mindlin and Cheng (1950)).

To the author knowledge this type of contact problem has not been solved explicitly in the published literature. The pressure distribution is usually assumed Hertzian; see for example Kabo and Ekberg (2002, 2005), or Courbon et al. (2005). Such an assumption could be made if the inclusion is located far from the surface. However, it will be shown here that the contact pressure distribution may be significantly modified by the presence of inhomogeneities close to the surface, which subsequently affect the subsurface stress distribution.

The effect of different parameters of the inhomogeneities was first investigated: their Young's modulus, Poisson's ratio, and radius. The test grid Table 1 summarizes the different arrangements chosen to study the influence of each parameter.

A cluster of spherical inhomogeneities is considered in a first example. The inhomogeneities are equally spaced into a domain constituted of $84 \times 84 \times 31$ cuboids such as the space between the inclusion centers is $\Delta x = \Delta y = \Delta z = 0.27a$ as shown in Fig. 4. This configuration includes 484 inclusions and the edge of a cuboid (mesh) is 0.2 μm. The radius of the inclusions is $r = 0.6$ μm $= 0.1 \times a$. Thus the total volume of inhomogeneities takes up 22% of the domain. The ratio of the inclusion Young's modulus to the matrix one is defined by the dimensionless parameter $\gamma = E_I/E_m$ whereas the Poisson's ratio is set constant $\nu_I = 0.3$.

Fig. 5 presents the dimensionless contact pressure distribution for various Young's modulus ratios γ ranging from 0 to 2. The contact pressure and x and y-coordinates are normalized by the Hertz pressure Po and contact radius a, respectively, which is the solution

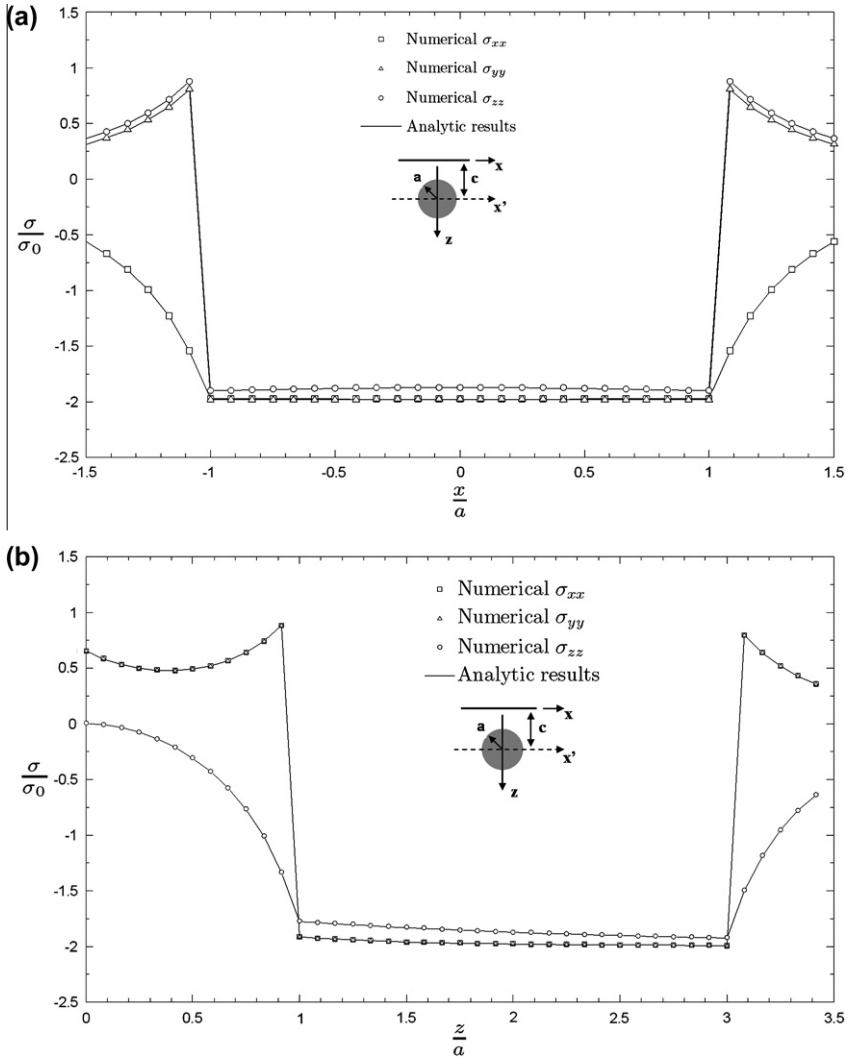

Fig. 2. Comparison between the analytical solution of Mindlin and Cheng (1950) and the present numerical solution for a spherical inclusion. Dimensionless stress along the x'-axis (a) and the z-axis (b).

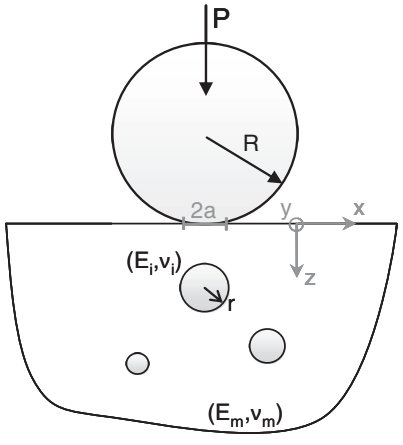

Fig. 3. Normal loading of a half-space containing multiple inclusions.

in the absence of inhomogeneity. It can be verified that the contact pressure distribution for a cluster of homogeneous inclusions (i.e. inhomogeneities with $\gamma = 1$) is equivalent to that of the homogeneous half-space (without inhomogeneity) which is the Hertz solution.

Fig. 6 shows the dimensionless pressure profile in the plane $y = 0$ for various ratios γ. It can be observed that, when the inclusion is softer than the half-space, i.e. $\gamma < 1$, the substrate material surrounding the inclusions becomes more compliant and the contact pressure gets smaller than the Hertzian pressure whereas the contact area increases. When the inclusions are stiffer than the matrix, the contact pressure exhibits peaks of magnitude higher than the solution without inclusion, and the contact area slightly decreases.

The maximum of the dimensionless contact pressure and von Mises stress are shown in Fig. 7 as function of the γ ratio. It can be seen that, when both Poisson's ratios equal 0.3, the maximum of the dimensionless contact pressure increases with the inclusion stiffness when the inclusions are stiffer than the matrix ($\gamma > 1$), whereas it remains almost constant and slightly lower than the homogeneous solution when inclusions are softer ($\gamma < 1$). An increase of more than 22% of the maximum contact pressure is found in this example when the Young's modulus of inhomogeneities is twice that of the matrix. Conversely the minimum of the dimensionless contact pressure decreases when decreasing the γ ratio for inclusions softer than the matrix, whereas it remains almost constant and slightly higher than the homogeneous solution for stiffer inclusions (see Fig. 6). Regarding the maximum von Mises stress, it is observed in Fig. 7 that either decreasing or increasing the inhomogeneity stiffness from the homogeneous solution in-

Table 1
Different configurations to study the influence of each inclusion parameters.

Inclusion parameter	Discretization mesh (cuboids)	Young's modulus ratio	Poisson's ratio	Radius r	Arrangement
Young's modulus	$84 \times 84 \times 31$	Variable $0 \leqslant \gamma \leqslant 2$	$\nu = 0.3$	$r = 0.1a$	3D-uniform distribution (484 inclusions)
Inclusion radius	$84 \times 84 \times 31$	$\gamma = 2$	$\nu = 0.3$	Variable $0.03 \leqslant \frac{r}{a} \leqslant 1.33$	One inclusion in two depth configurations
Poisson's ratio	$84 \times 84 \times 31$	$\gamma = 0.5, \gamma = 2$	Variable $0 \leqslant \nu \leqslant 0.45$	$r = 0.1a$	3D-uniform distribution (484 inclusions)
Depth	$84 \times 84 \times 31$	$\gamma = 2$	$\nu = 0.3$	$r = 0.13a$	2D-uniform distribution (49 inclusions)

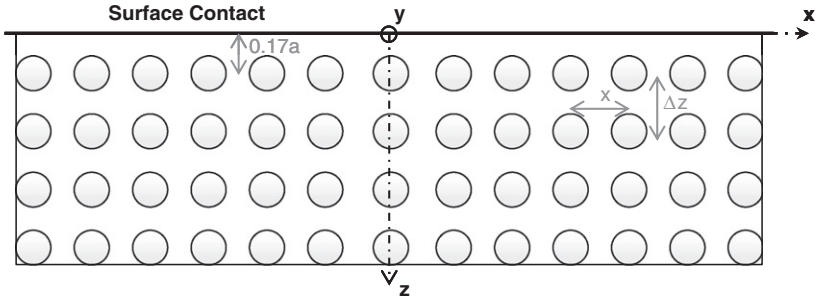

Fig. 4. Representation of the inclusion pattern in the (Oxz) plane.

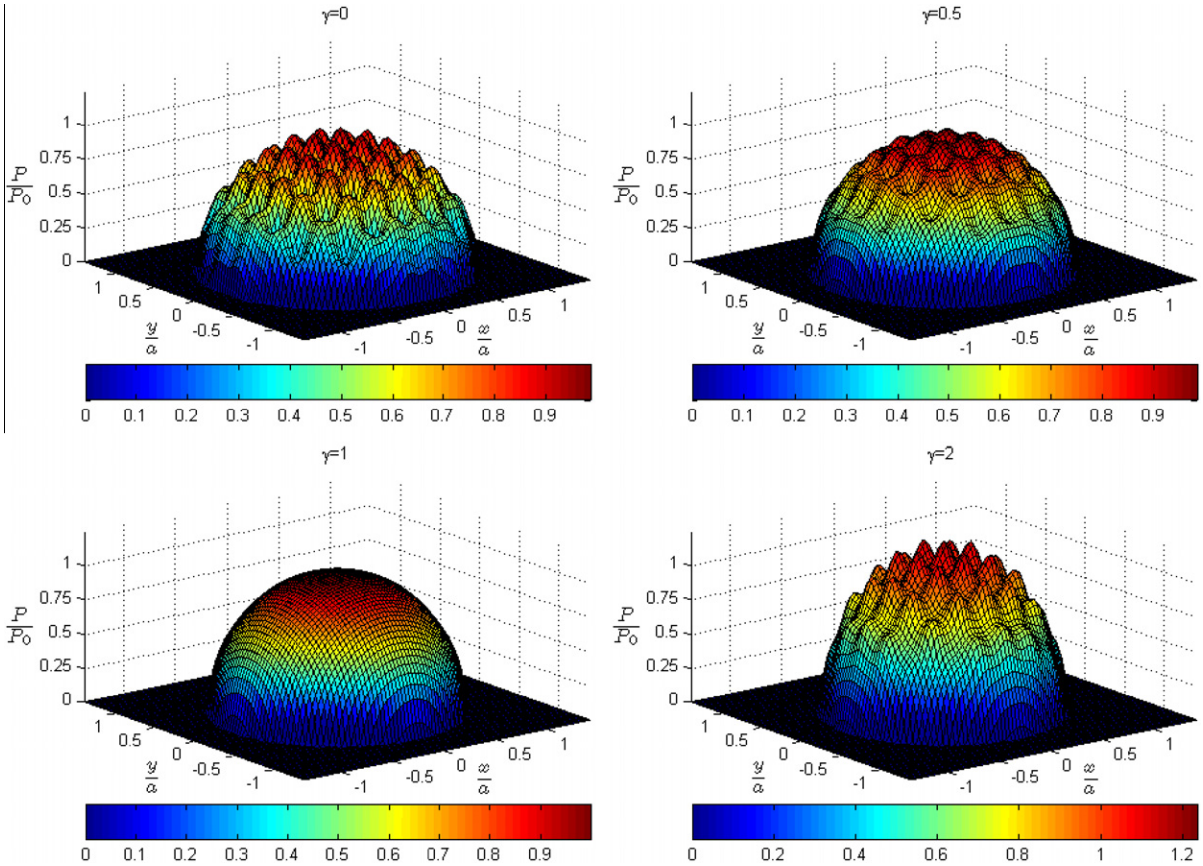

Fig. 5. Contact pressure distribution for inhomogeneities of various stiffnesses ($\gamma = 0, 0.5, 1, 2$).

creases the stress magnitude. The dimensionless von Mises stress reaches 0.94 for $\gamma = 2$ (i.e. stiff inclusion) and 1.18 when $\gamma = 0$ (void). Note that the maximum of the dimensionless von Mises stress is found minimum for $\gamma = 1$, i.e. $\sigma/Po = 0.62$, which corresponds to the Hertzian or homogeneous solution at depth $z/a = 0.481$.

The effect of a single spherical inhomogeneity located near the surface and with its center lying along the axis of symmetry as shown in Fig. 8 is now investigated. As shown schematically two situations can be encountered. In Fig. 8(a) one point of the inhomogeneity surface is always tangent to the contact surface and the center of the inhomogeneity is located at $(0,0,r)$. In Fig. 8(b) the

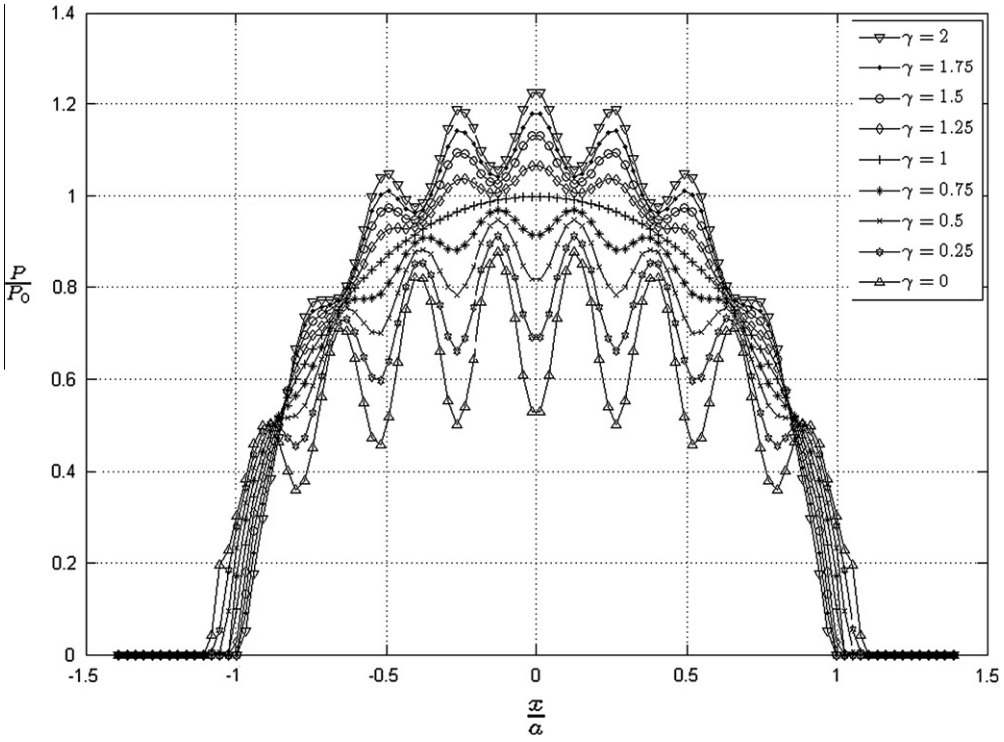

Fig. 6. Contact pressure profile for inhomogeneities of various stiffnesses ($\gamma = 0$–2).

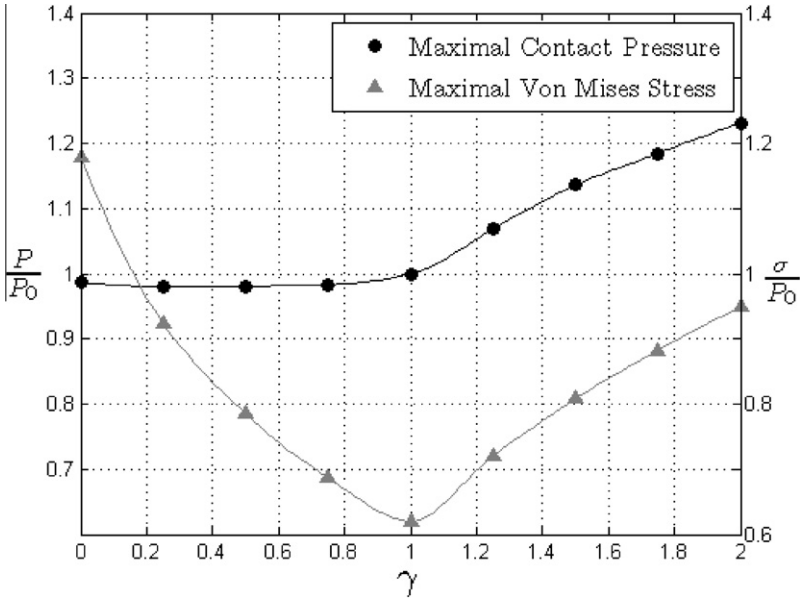

Fig. 7. Maximum dimensionless contact pressure and von Mises stress vs. the ratio $\gamma = E_i/E_m$.

center of the inhomogeneity is kept fixed and located at $(0,0,h = 0.5 \times a)$ which is close for a circular contact with homogeneous material to the point where the von Mises stress is found maximum. Note that in the current example the Poisson's ratios and the Young's modulus ratio are $v = 0.3$ and $\gamma = 2$, respectively.

Fig. 9 presents the profile of the dimensionless contact pressure in the plane $y = 0$ for different inclusion radii when they are tangent to the surface, see Fig. 8(a). The same profile is shown in Fig. 10 when the inclusion center remains fixed, see Fig. 8(b). It is obvious that the presence of an inhomogeneity in the vicinity of the contact strongly affects the contact pressure distribution. For inclusions tangent to the contact surface effects are significant even for small radius; $r = 0.03 \times a$ implies an increase of the contact pressure of nearly 25%. For inhomogeneities located at the Hertzian depth the effect on the contact pressure becomes significant for $r = 0.17 \times a$ and larger radius. Fig. 11 shows the maximum dimensionless contact pressure and von Mises stress for different values of radius r for configurations (a) and (b) in Fig. 8. For configuration (a), the maximum contact pressure is found maximum and equal to $P_{max} = 1.75 \times Po$ for $r = 0.17 \times a$, whereas the maximum von Mises stress is found for $0.33 \times a < r < 0.67 \times a$. For configuration (b) i.e. when the inclusion center is maintained fixed, one ob-

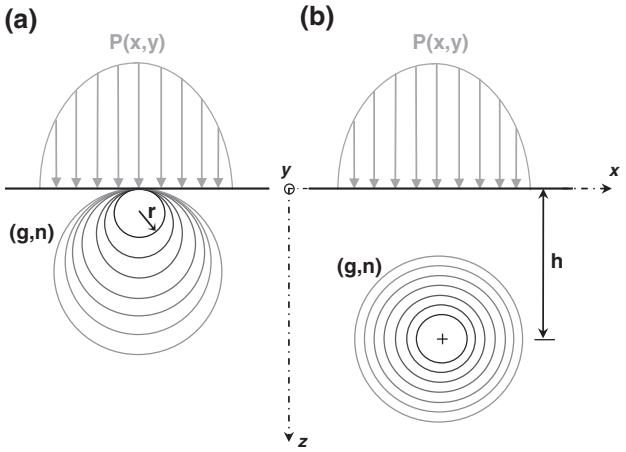

Fig. 8. Schematic representation of two configurations to study the influence of the inhomogeneity of various radius r. Note that the size of the inclusion relatively to the contact radius is magnified for visibility. (a) The inhomogeneity is always tangent to the surface then the location of its center is varying and (b) the center of the inhomogeneity is fixed at depth $h = 0.5 \times a$.

serves a monotonic increase of the contact pressure and von Mises stress with the radius of the inhomogeneity. A soft inclusion will lead to a reduction of the contact pressure in a similar manner.

When several inhomogeneities are present the solution may be affected by the interactions between them. Fig. 12 shows the distribution of the contact pressure for a cluster of spherical inhomogeneities. Here all neighboring inclusions of same radius $r = 0.17 \times a$ are tangent to the contact surface. It is observed that the maximum of the contact pressure ($P_{max} = 1.65 \times Po$) becomes slightly lower compared to the case of a single inhomogeneity ($P_{max} = 1.75 \times Po$) whereas the maximum of the von Mises stress slightly increases from $\sigma_{max} = 0.92 \times Po$ to $\sigma_{max} = 0.99 \times Po$.

The effect of the Poisson's ratio is now analyzed. A cluster of spherical inhomogeneities equally spaced within a domain composed of $84 \times 84 \times 31$ cuboids such that the inclusion centers is $\Delta x = \Delta y = \Delta z = 0.27a$ is considered, giving 484 inclusions. The size (edge) of each cuboid is 0.2 μm. The radius of the inclusions is $r = 0.6$ μm $= 0.1 \times a$. Thus the inhomogeneities take up 22% of the volume within the domain of interest (no inclusion is considered far away from the contact). Fig. 13 shows the dimensionless maximum of the contact pressure and von Mises stress with different Poisson's ratios for relatively compliant ($\gamma = 0.5$) and stiff inhomogeneities ($\gamma = 2$). For stiff inclusions ($\gamma = 2$), the maximum of the contact pressure is not too much influenced by the variation of the Poisson's ratio except for nearly incompressible ones ($\nu = 0.45$) that produces an increase of the contact pressure of nearly 28% on the top of each of them. Meantime the maximum von Mises stress decreases continuously when the Poisson's ratio increases. For relatively soft inclusions ($\gamma = 0.5$) the maximum contact pressure is independent of the Poisson's ratio – in fact only the minimum of the pressure distribution is influenced, see Fig. 14. More surprisingly, it can be observed that, in term of von Mises stress, the worst situation for a soft inclusion is when they are nearly incompressible ($\sigma/Po = 1.09$ for $\nu = 0.45$).

The effect of the depth h of a horizontal plane of inhomogeneities is now investigated. A set of 49 inclusions equally spaced in a zone composed of 84×84 cuboids is considered such as the distance between inclusion centers is $\Delta x = \Delta y = 0.37a$. The edge of a cuboid is 0.2 μm. The inhomogeneities with Young's modulus ratio $\gamma = 2$ and Poisson's ratio $\nu = 0.3$ have a radius $r = 0.8$ μm $= 0.13 \times a$. Fig. 15 shows the effects of the plane depth on the contact pressure profile in the plane $y = 0$. The pressure fluctuation becomes significant when the inclusions are located at a depth lower than $0.3 \times a$, and reaches a maximum when they are tangent to the contact surface (i.e. for $h = 0.87 \times a$). Fig. 16 shows the influence of the depth h where inhomogeneities are located on the maximum contact pressure and von Mises stress. Obviously the influence of inhomogeneities on the contact pressure diminishes as the inhomogeneities move away from the contact surface. When $h/a > 0.4$, the effect of the inhomogeneities on contact pressure becomes insignificant and the distribution of contact pressure converges to the solution

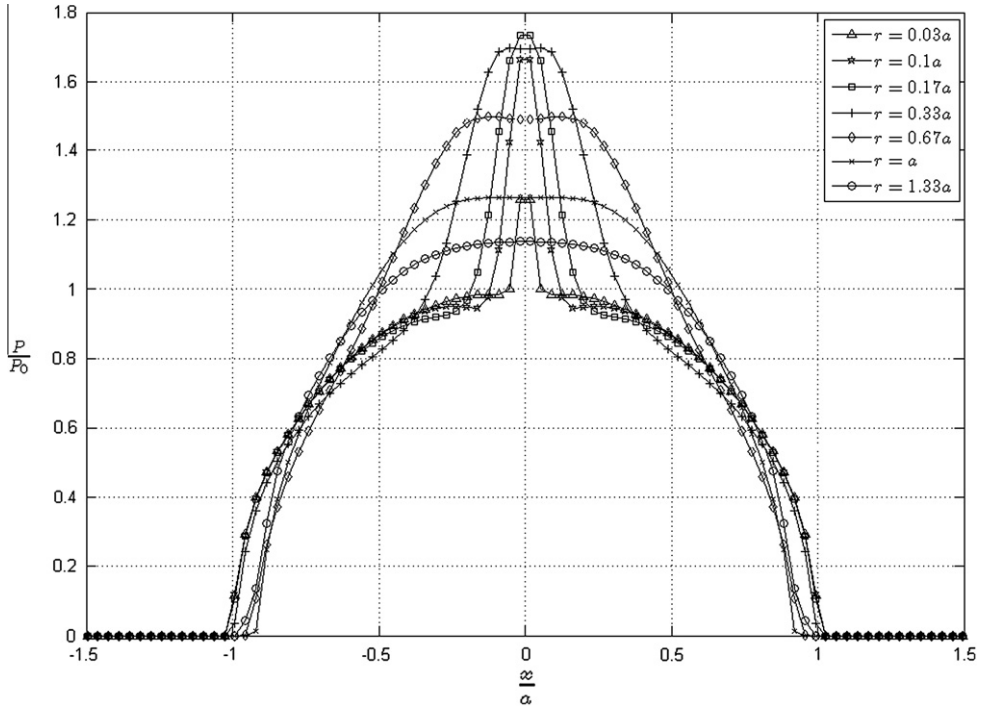

Fig. 9. Contact pressure profile in the plane $y = 0$ for an inhomogeneity ($\nu = 0.3$ and $\gamma = 2$) of different radii and tangential to the surface, cf. Fig. 8(a).

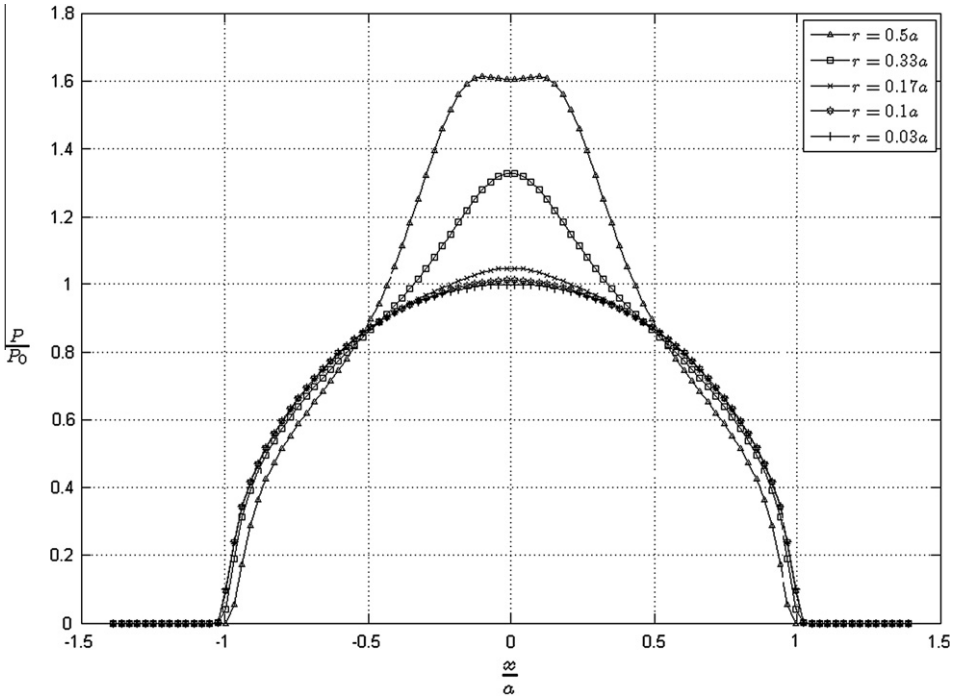

Fig. 10. Contact pressure profile in the plane $y = 0$ for an inhomogeneity ($\nu = 0.3$ and $\gamma = 2$) of different radii at depth $h = 0.5 \times a$, cf. Fig. 8(b).

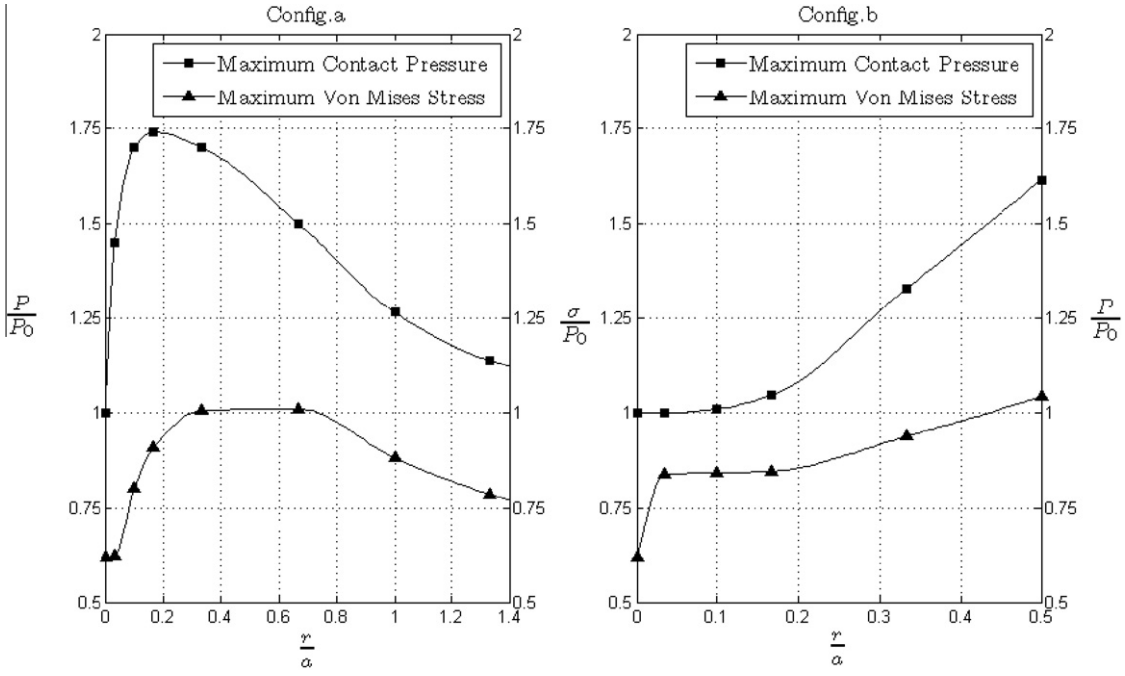

Fig. 11. Maximum contact pressure and von Mises stress vs. the inclusion radius.

of homogeneous half-space. The pressure peak reaches $1.75 \times Po$ when the inclusions are tangent to the surface ($\gamma = 2, \nu = 0.3$). Note that the maximum von Mises stress is found for $h/a \cong 0.5$ which is coherent with the Hertz solution. To look more closely on how nearby inclusions interact only two of them will be now considered.

The interaction between inhomogeneities is another factor that significantly affects the location and magnitude of the maximum von Mises stress. It can be noted that the interaction can be neglected when the spacing between the center of two close inclusions becomes larger than four times their radius. The influence of neighboring inclusions is studied here by considering two spherical inclusions in the elastic half-space as shown in Fig. 17, one of them (inclusion numbered 1) being lying along the z-axis which is the axis of symmetry normal to the circular contact area. The inhomogeneities have the same Poisson's ratio $\nu = 0.3$ and the same radius $r = 0.13 \times a$. The centers of two inhomogeneities are separated by a distance d. The variable d is formulated through the dimensionless distance β such as $\beta = \frac{d-2r}{r}$. $\beta = 0$ means that the two inclusions are in contact ($\beta \in [0, \infty[$).

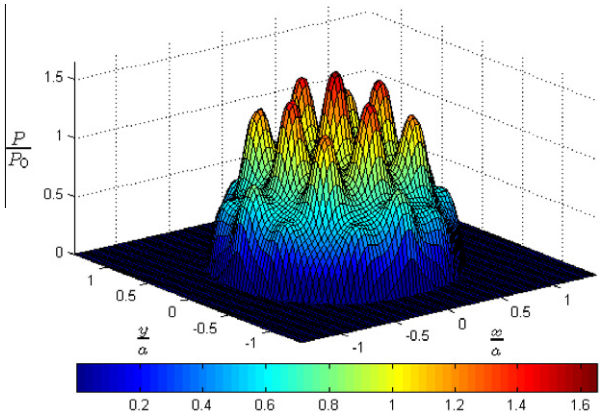

Fig. 12. Distribution of the contact pressure for a cluster of spherical inhomogeneities tangent to the contact surface.

Fig. 18 shows the contact pressure profile for different combinations of Young's modulus relatively to the matrix, i.e. $\gamma_1 = 0.5$ and 2 and $\gamma_2 = 0$, 0.5, and 2. Here the inclusions are separated by the distance $\beta = 0.25$ at the depth $h = 0.23 \times a$. For reference, the Hertzian solution is also plotted. It is shown that, independently of the stiffness of the first inhomogeneity, the peak or dip of the contact pressure on the top of this first inhomogeneity is hardly affected by the presence of a second one when located in the same horizontal plane, including when inclusions are relatively close (here $\beta = 0.25$). It could be concluded that the effect of neighboring inclusions on the contact pressure above a first one is quite limited, when they are located at the same depth. Conversely an alignment of inclusions along the vertical direction will affect the pressure distribution on the top of the stringer.

The mismatch of material properties could induce sliding failure at the interface between the inclusions and the matrix. The region where the maximum shear stress is located could also give birth to fatigue cracks. Fig. 19 shows the influence of the spacing between the two inclusions located at depth $h = 0.23 \times a$ for different ratios of their Young's modulus normalized by the matrix value (γ_1, γ_2) on the maximum shear stress evaluated at point P located at coordinates $(r, 0, 0.23 \times a)$. For comparison, the maximum shear stress for a single inclusion is also included in the form of a dash line. It is shown that the maximum shear stress starts to be significantly affected when the dimensionless spacing β is lower than 3. Note that, when both a soft and a stiff inclusion are present, the shear stress decreases and increases near the soft and stiff inclusion, respectively. It can be also noticed that the maximum shear stress tends to increase at point P when two inclusions softer than the matrix become closer. Conversely the maximum stress is relaxed near the inclusion interface when both interacting inclusions are stiffer than the matrix. Finally the worst situation is found in presence of voids or cavities ($\gamma = 0$), particularly when they are located near stiff inhomogeneities ($\tau_m/Po = 0.54$ for $\beta = 0.25$, $\gamma_1 = 2$ and $\gamma_2 = 0$, see right plot in Fig. 19).

It should be recalled that for a circular point contact the maximum shear stress is located at depth $h = 0.5 \times a$ ($0.48 \times a$ accurately), whereas the two interacting inclusions have been previously located at depth $h = 0.23 \times a$ only in order to strongly affect the contact pressure distribution which is no more Hertzian. Fig. 20 shows similar results as in Fig. 19 except that the two inclusions are now located at depth $h = 0.5 \times a$ and the stress given at point P' located at the coordinates $(r, 0, 0.5 \times a)$. It is found that, when $3 < d/r < 5$ and for two inclusions softer than the matrix, the magnitude of the maximum shear stress increases slightly compared to the case of a single inclusion. When $d/r < 3$ (i.e. $\beta < 1$), the soft inclusion relaxes the surrounding material and reduces the magnitude of maximum shear stress. On the other hand, the effect of stiff inclusion could cause the maximum shear stress to increase as the distance between the inclusions decreases. The very different behaviors of the interactions between two close inhomogeneities as plotted in Figs. 19 and 20 could be explained first by the contact pressure distribution on the top of inclusions.

It should be mentioned that the sharp strain gradient at the interface between the inclusion and the matrix as pointed out by Benedikt et al. (2006) is not considered by the Eshelby's equivalent inclusion method. It affects a very small volume in the vicinity of the interface that may modify the solution for interacting inclusions when they are very close each other. The compatibility strain concentrated in the zone very close to the interface, generating high strain gradient, has been recently studied by Benedikt et al.

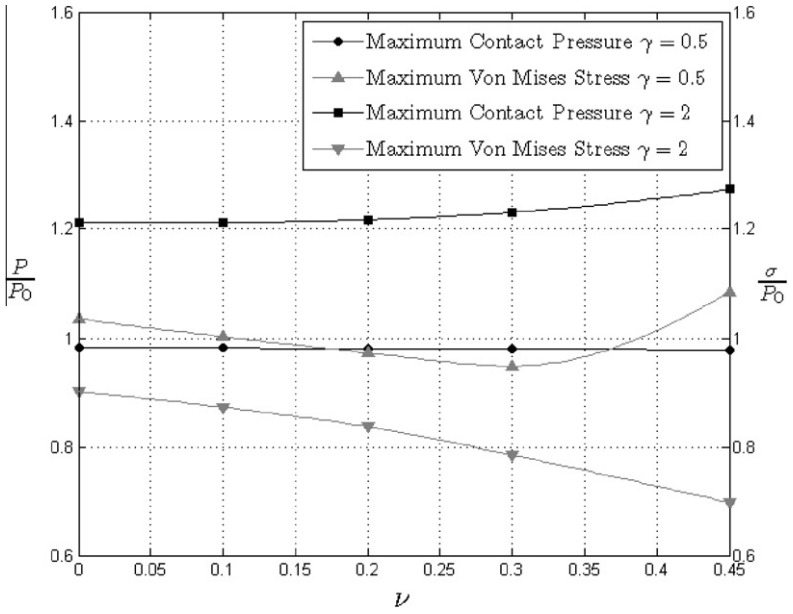

Fig. 13. Maximum contact pressure and von Mises stress vs. the inclusion Poisson's ratio.

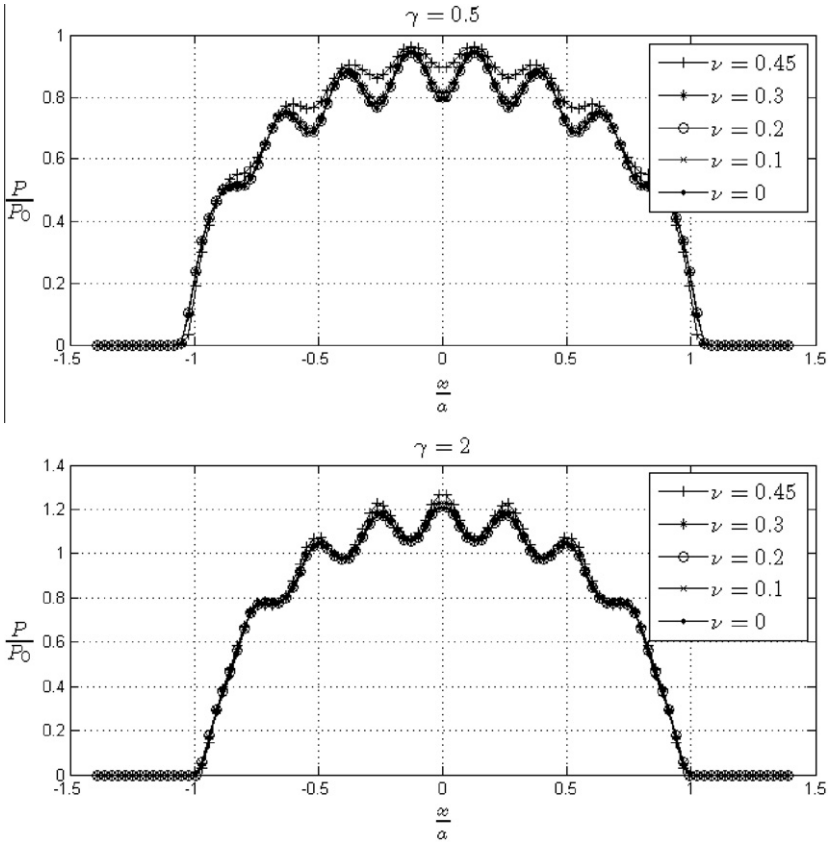

Fig. 14. Profile of the contact pressure in the plane $y = 0$ for soft or stiff inhomogeneities for various inclusion Poisson's ratio ($\nu_m = 0.3$).

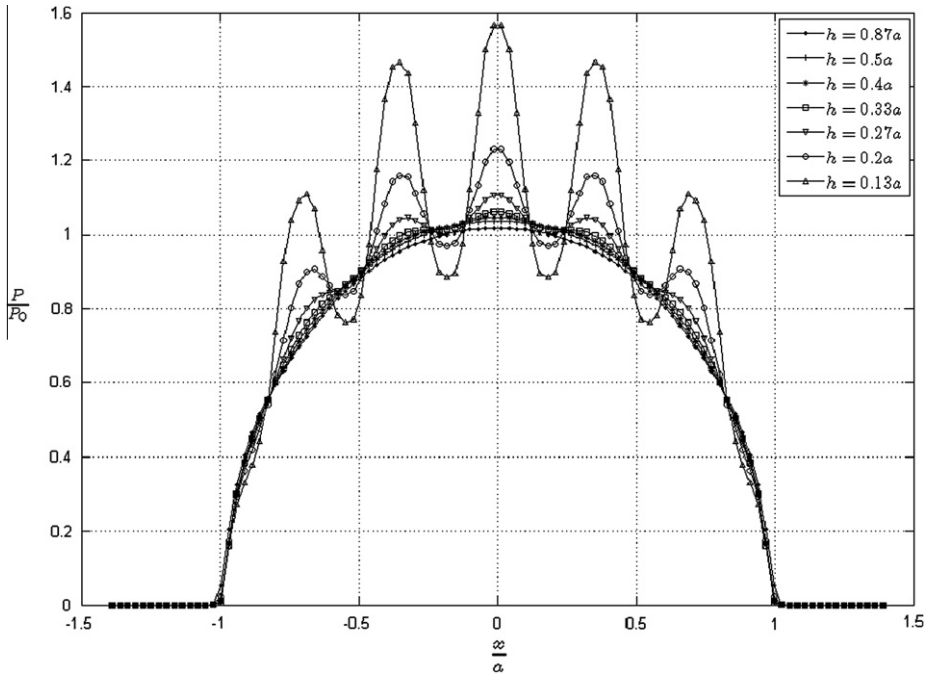

Fig. 15. Profile of the contact pressure in the plane $y = 0$ for a set of 49 inhomogeneities equally spaced in a horizontal plane at depth h.

(2006). They presented a three-dimensional stress analysis around interacting spherical inclusions, using a Taylor series expansion to find the approximate solution of equivalent method equations with constant, linear, or quadratic eigenstrains. They concluded that the quadratic expansion order of the constrained strain and eigenstrains allows to reduce the error between the equivalent inclusion method and the finite element solution for two close inhomogeneities. This development has not yet been included in

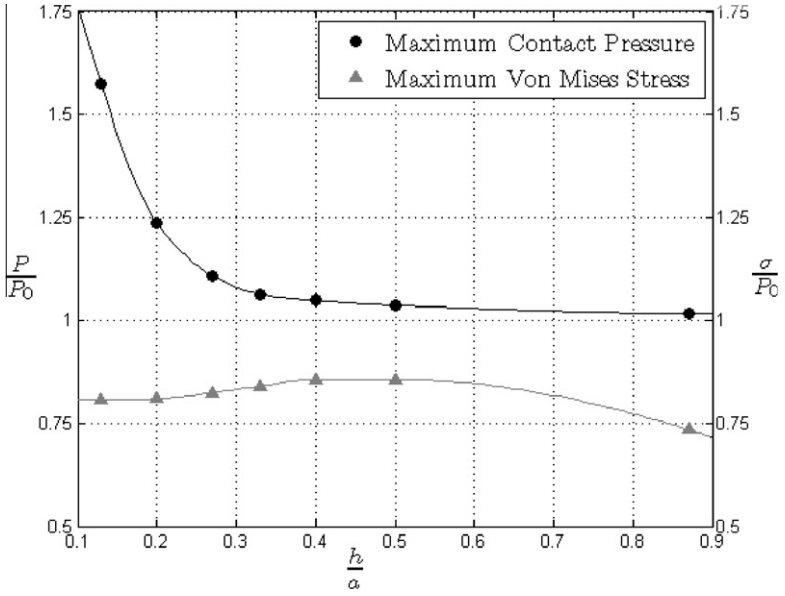

Fig. 16. Maximum contact pressure and von Mises stress as a function of the depth where inclusions are located.

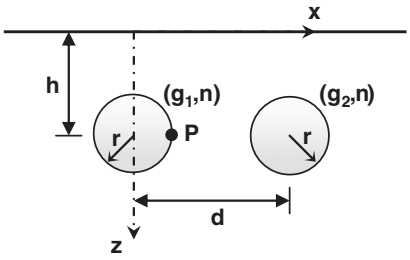

Fig. 17. Representation of two inhomogeneities in the elastic half-space.

the present model but constitutes one of the perspectives of this work.

4. Conclusion

This paper presents the main features of a fast semi-analytical three-dimensional method to treat the contact problem for a half-space containing multiple inhomogeneities. Analytical Eshelby solutions have been implemented in the contact solver to account for spherical inhomogeneities. It can be seen as a method to enrich the classical homogeneous solution of the contact problem. This technique is highly efficient in terms of computing time. The numerical results given underline that most of the time it is not correct to assume a Hertzian pressure distribution for the contact problem in presence of soft or stiff inhomogeneities near the contacting surface, since the pressure distribution may exhibits peak of pressure with a magnitude up to 1.75 times the Hertz solution. The peaks of pressure are located above stiff inhomogeneities while soft ones produce a local decrease of the contact pressure compared with that for the homogeneous half-space. The Poisson's ratio is also an important parameter which could increase significantly the contact pressure on the top of inhomogeneities when they tend to be incompressible (for example a cavity filled with a liquid). It is also noted that stiff inhomogeneity acts to toughen the surrounding material and reduce subsurface stress at the inclusion-matrix interface. This phenomenon is amplified when the

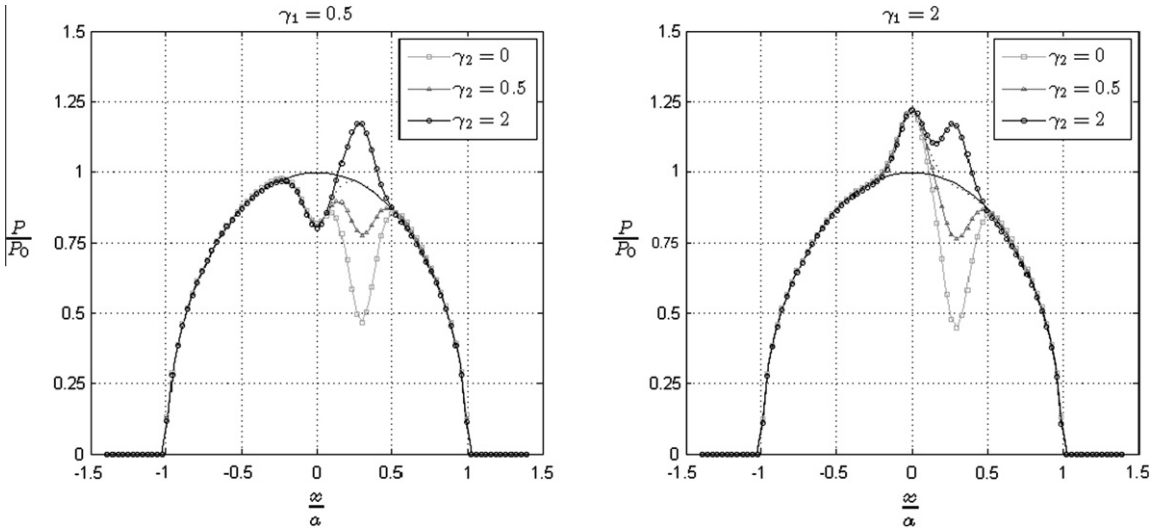

Fig. 18. Profile of the contact pressure on the top of two inclusions of various stiffnesses (γ_1 and γ_2).

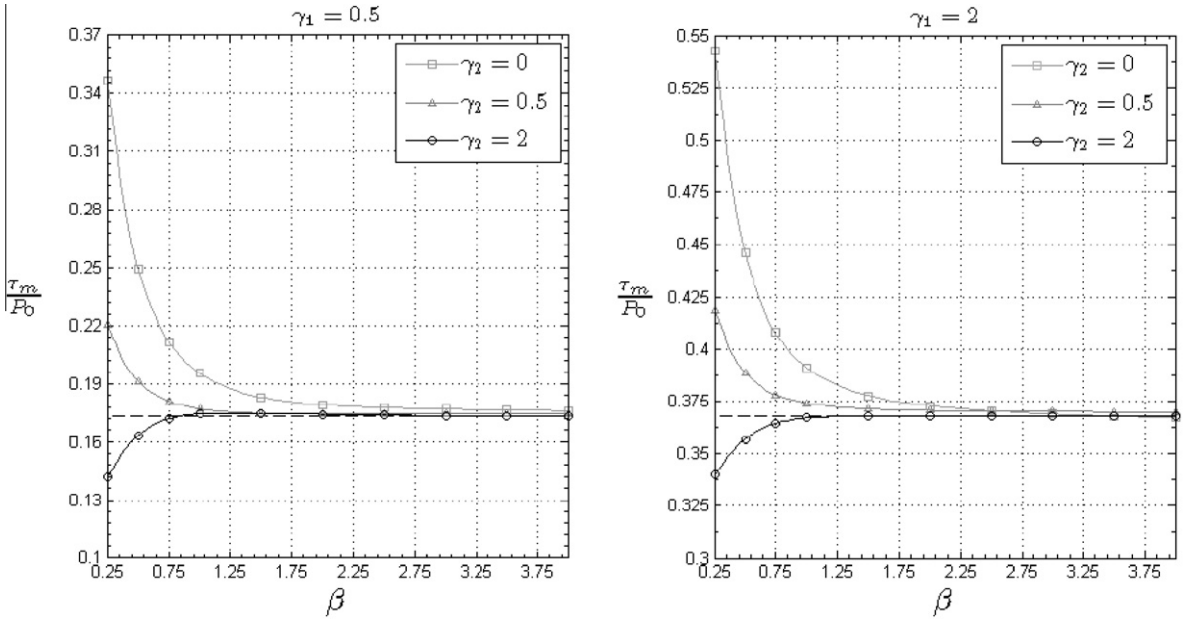

Fig. 19. Maximum shear stress at point P of coordinate $(r, 0, 0.23 \times a)$ as a function of the spacing between the two inclusions located at depth $h = 0.23 \times a$.

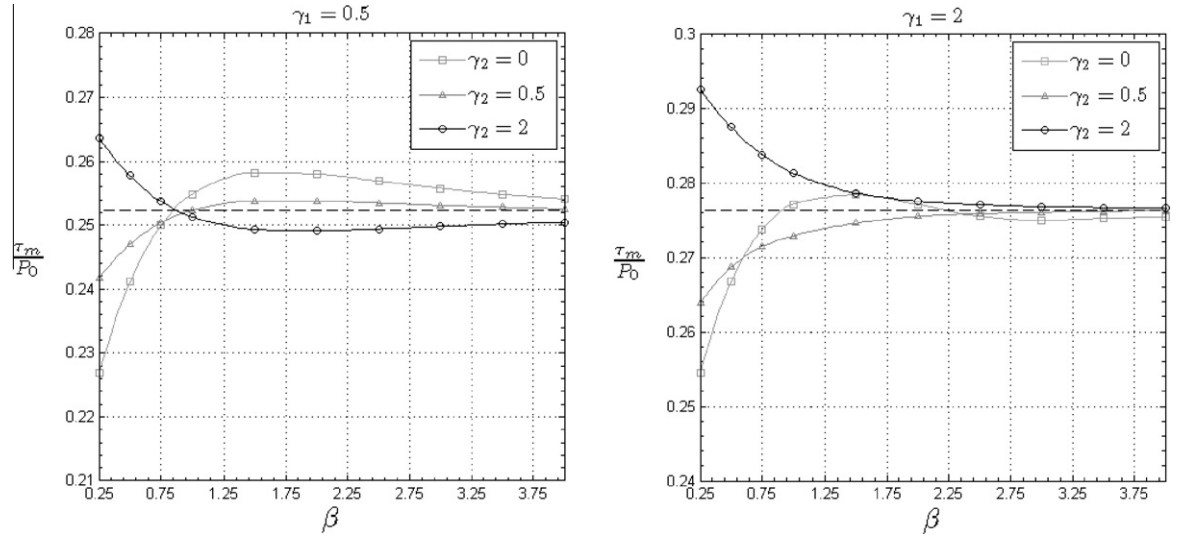

Fig. 20. Maximum shear stress at point P' of coordinate $(r, 0, 0.5 \times a)$ as a function of the spacing between the two inclusions located at depth $h = 0.5 \times a$.

inhomogeneities get closer. A list of the most important results is given below:

1. The pressure fluctuation becomes significant when the inclusions are located at a depth h lower than $0.3 \times a$, a being the Hertz contact radius, and reaches a maximum when they are tangent to the contact surface. When $h/a > 0.4$, the effect of the inhomogeneities on the contact pressure becomes insignificant and the distribution of contact pressure converges to the solution of homogeneous half-space.
2. For stiff inhomogeneities of Young's modulus two times the matrix one ($\gamma = 2$), and Poisson's ratio of 0.3 also identical to those of the matrix, the peak of pressure may reach up to $1.75 \times Po$, Po being the Hertz contact pressure, when the inclusions are tangent to the surface.
3. The contact pressure on the top of an inhomogeneity is hardly affected by neighbours ones when they are located in the same plane parallel to the contact surface, including when they are very close.
4. The Poisson's ratio of the inhomogeneities has a strong influence on the pressure distribution when it tends to the incompressible case ($\nu = 0.5$).
5. The presence of a soft inclusion close to a stiff one significantly increases the local stress nearby the hard inclusion. A concentration factor of nearly 2 ($\tau_m/Po = 0.54$ for $\beta = 0.25$, $\gamma_1 = 2$ and $\gamma_2 = 0$) can be found when a void is located nearby a stiff one ($\gamma = 2$) at mid-way ($z = 0.23 \times a$) between the Hertzian depth ($z = 0.48 \times a$) and the surface, compared to the homogeneous Hertz solution ($\tau_m/Po = 0.3$ at $z = 0.48 \times a$).

Appendix A. Stresses in a half-space due to the concentrated unit normal force at the surface origin (F_{ij})

$$
\begin{aligned}
F_{11}(x_1,x_2,x_3) &= \frac{1}{2\pi}\left[\frac{1-2\nu}{r^2}\left\{\left(1-\frac{x_3}{\rho}\right)\frac{x_1^2-x_2^2}{r^2}+\frac{x_3x_2^2}{\rho^3}\right\}-\frac{3x_3x_1^2}{\rho^5}\right],\\
F_{22}(x_1,x_2,x_3) &= F_{11}(x_2,x_1,x_3),\\
F_{33}(x_1,x_2,x_3) &= -\frac{3}{2\pi}\frac{x_3^3}{\rho^5},\\
F_{12}(x_1,x_2,x_3) &= \frac{1}{2\pi}\left[\frac{1-2\nu}{r^2}\left\{\left(1-\frac{x_3}{\rho}\right)\frac{x_1x_2}{r^2}+\frac{x_3x_2x_1}{\rho^3}\right\}-\frac{3x_3x_2x_1}{\rho^5}\right],\\
F_{12}(x_1,x_2,x_3) &= -\frac{3}{2\pi}\frac{x_1x_3^2}{\rho^5},\\
F_{23}(x_1,x_2,x_3) &= F_{12}(x_2,x_1,x_3),
\end{aligned}
\tag{A1}
$$

where

$$r^2 = x_1^2+x_2^2, \quad \rho = \sqrt{x_1^2+x_2^2+x_3^2},$$

with ν, the Poisson's ratio of the isotropic half-space.

Appendix B. Stresses in a half-space subject to normal pressure (M_{ij})

An isotropic half-space is subjected to an uniform normal pressure σ_n in a discretized surface area of $2\Delta x_1 \times 2\Delta x_2$ at the center point $P(x_1', x_2', 0)$. The stress at an observation point $Q(x_1,x_2,x_3)$ is given by Zhou et al. (2009) and Johnson (1985):

$$
\begin{aligned}
\sigma_{ij}(x_1,x_2,x_3) &= M_{ij}(x_1-x_1',x_2-x_2',x_3)\sigma_n(x_1,x_2),\\
\sigma_{ij}(x_1,x_2,x_3) &= \frac{\sigma_n}{2\pi}\left[\begin{array}{l} h_{ij}(\xi_1+\Delta x_1,\xi_2+\Delta x_2,\xi_3)-h_{ij}(\xi_1+\Delta x_1,\xi_2-\Delta x_2,\xi_3)\\ +h_{ij}(\xi_1-\Delta x_1,\xi_2-\Delta x_2,\xi_3)-h_{ij}(\xi_1-\Delta x_1,\xi_2+\Delta x_2,\xi_3)\end{array}\right],
\end{aligned}
\tag{B1}
$$

where

$$\xi_i = x_i - x_i'.$$

The functions $h_{ij}()$ in Eq. (B1) are defined by

$$
\begin{aligned}
h_{11}(x_1,x_2,x_3) &= 2\nu\tan^{-1}\frac{x_2^2+x_3^2-\rho x_2}{x_1x_3}\\
&\quad +2(1-\nu)\tan^{-1}\frac{\rho-x_2+x_3}{x_1}+\frac{x_1x_2x_3}{\rho(x_1^2+x_3^2)},\\
h_{22}(x_1,x_2,x_3) &= h_{11}(x_2,x_1,x_3),\\
h_{33}(x_1,x_2,x_3) &= \tan^{-1}\frac{x_2^2+x_3^2-\rho x_2}{x_1x_3}-\frac{x_1x_2x_3}{\rho}\left(\frac{1}{x_1^2+x_3^2}+\frac{1}{x_2^2+x_3^2}\right),\\
h_{12}(x_1,x_2,x_3) &= -\frac{x_3}{\rho}-(1-2\nu)\log(\rho+x_3),\\
h_{13}(x_1,x_2,x_3) &= \frac{x_2x_3^2}{\rho(x_1^2+x_3^2)},\\
h_{23}(x_1,x_2,x_3) &= h_{13}(x_2,x_1,x_3),
\end{aligned}
\tag{B2}
$$

where

$$\rho = \sqrt{x_1^2+x_2^2+x_3^2}.$$

Appendix C. Normal displacement at the interface subject to normal pressure (K^n)

Consider the contact between a sphere and an elastic half-space with elastic constants (E_1,ν_1) and (E_2,ν_2), respectively. The contact surface $x_3 = 0$ is discretized into rectangular surface areas of $2\Delta_1 \times 2\Delta_2$. The origin of the Cartesian coordinate system (x_1,x_2,x_3) is set to be the initial contact point. The normal displacement at an observation point $P(\xi_1,\xi_2,0)$ is related to the pressure field at the center $Q = (\xi_1',\xi_2',0)$ by the function K^n

$$K^n(c_1,c_2) = \left[\frac{1-\nu_1^2}{\pi E_1}+\frac{1-\nu_2^2}{\pi E_2}\right]\sum_{p=1}^{4}K_p^n(c_1,c_2), \tag{C1}$$

$$
\begin{aligned}
K_1^n(c_1,c_2) &= (c_1+\Delta_1)\log\left(\frac{(c_2+\Delta_2)+\sqrt{(c_2+\Delta_2)^2+(c_1+\Delta_1)^2}}{(c_2-\Delta_2)+\sqrt{(c_2-\Delta_2)^2+(c_1+\Delta_1)^2}}\right),\\
K_2^n(c_1,c_2) &= (c_2+\Delta_2)\log\left(\frac{(c_1+\Delta_1)+\sqrt{(c_2+\Delta_2)^2+(c_1+\Delta_1)^2}}{(c_1-\Delta_1)+\sqrt{(c_2+\Delta_2)^2+(c_1-\Delta_1)^2}}\right),\\
K_3^n(c_1,c_2) &= (c_1-\Delta_1)\log\left(\frac{(c_2-\Delta_2)+\sqrt{(c_2-\Delta_2)^2+(c_1-\Delta_1)^2}}{(c_2+\Delta_2)+\sqrt{(c_2+\Delta_2)^2+(c_1-\Delta_1)^2}}\right),\\
K_4^n(c_1,c_2) &= (c_2-\Delta_2)\log\left(\frac{(c_1-\Delta_1)+\sqrt{(c_2-\Delta_2)^2+(c_1-\Delta_1)^2}}{(c_1+\Delta_1)+\sqrt{(c_2-\Delta_2)^2+(c_1+\Delta_1)^2}}\right),
\end{aligned}
\tag{C2}
$$

where, $c_1 = \xi_1 - \xi_1'$ and $c_2 = \xi_2 - \xi_2'$.

References

Aderogba, K., 1976. On eigenstresses in a semi-infinite solid. Mathematical Proceedings of the Cambridge Philosophical Society 80 (3), 555–562.

Antaluca, E., Nélias, D., 2008. Contact fatigue analysis of a dented surface in a dry elastic-plastic circular point contact. Tribology Letters 29 (2), 139–153.

Asaro, R.J., Barnett, D.M., 1975. The nonuniform transformation strain problem for an anisotropic ellipsoidal inclusion. Journal of the Mechanics of Physics and Solids 23, 77–83.

Benedikt, B., Lewis, M., Rangaswamy, P., 2006. On elastic interactions between spherical inclusions by the equivalent inclusion method. Computational Materials Science 37, 380–392.

Boucly, V., Nélias, D., Liu, S., Wang, Q.J., Keer, L.M., 2005. Contact analyses for bodies with frictional heating and plastic behaviour. ASME Journal of Tribology 127 (2), 355–364.

Chen, W.W., Wang, Q., 2008. Thermomechanical analysis of elasto-plastic bodies in a sliding spherical contact and the effects of sliding speed, heat partition, and thermal softening. ASME Journal of Tribology 130, 041402-1–041402-10.

Chen, W.W., Wang, Q., 2009. A numerical static friction model for spherical contacts of rough surfaces, influence of load, material, and roughness. ASME Journal of Tribology 131, 021402-1–021402-8.

Chen, W.W., Wang, Q., Liu, Y., Chen, W., Cao, J., Xia, C., Talwar, R., Lederich, R., 2007. Analysis and convenient formulas for elasto-plastic contacts of nominally flat surfaces: average gap, contact area ratio, and plastically deformed volume. Tribology Letters 28, 27–38.

Chen, W.W., Liu, S.B., Wang, Q., 2008a. FFT-based numerical methods for elasto-plastic contacts of nominally flat surfaces. ASME Journal of Applied Mechanics 75, 011022-1–011022-11.

Chen, W.W., Wang, Q., Wang, F., Keer, L.M., Cao, J., 2008b. Three-dimensional repeated elasto-plastic point contact, rolling and sliding. ASME Journal of Applied Mechanics 75, 021021-1–021021-12.

Chen, W.W., Kim, W., Wang, Q., 2009. Transient thermomechanical analysis of sliding electrical contact of elasto-plastic bodies, thermal softening and melting inception. ASME Journal of Tribology 131, 021406-1–021406-10.

Chiu, Y.P., 1977. On the stress field due to initial strains in a cuboid surrounded by an infinite elastic space. ASME Journal of Applied Mechanics 44, 587–590.

Chiu, Y.P., 1978. On the stress field and surface deformation in a half space with a cuboidal zone in which initial strains are uniform. ASME Journal of Applied Mechanics 45, 302–306.

Courbon, J., Lormand, G., Dudragne, G., Daguier, P., Vincent, A., 2005. Influence of inclusion pairs, clusters and stringers on the lower bound of the endurance limit of bearing steels. Tribology International 36, 921–928.

Edward, R.H., 1951. Stress concentrations around spheroidal inclusions and cavities. ASME Journal of Applied Mechanics 18, 19–30.

Eshelby, J.D., 1957. The determination of the elastic field of an ellipsoidal inclusion and related problems. In: Proceedings of the Royal Society of London, A241, pp. 376–396.
Eshelby, J.D., 1959. The elastic field outside an elastic inclusion. In: Proceedings of the Royal Society of London, A252, pp. 561–569.
Eshelby, J.D., 1961. Elastic inclusions and inhomogeneities. In: Sneddon, L.N., Hill, R. (Eds.), Progress in Solid Mechanics, vol. 2. North-Holland, Amsterdam, pp. 89–140.
Fulleringer, B., Nélias, D., 2010. On the tangential displacement of a surface point due to a cuboid of uniform plastic strain in a half-space. ASME Journal of Applied Mechanics 77 (2), 021014-1–021014-7.
Gallego, L., Nélias, D., 2007. Modeling of fretting wear under gross slip and partial slip conditions. ASME Journal of Tribology 129 (3), 528–535.
Gallego, L., Nélias, D., Jacq, C., 2006. A comprehensive method to predict wear and to define the optimum geometry of fretting surfaces. ASME Journal of Tribology 128 (3), 476–485.
Gallego, L., Fulleringer, B., Deyber, S., Nélias, D., 2010. Multiscale computation of fretting wear at the blade/disk interface. Tribology International 43, 708–718.
Gallego, L., Nélias, D., Deyber, S., 2010. A fast and efficient contact algorithm for fretting problems applied to fretting modes I, II and III. Wear 268, 208–222.
Jacq, C., Nélias, D., Lormand, G., Girodin, D., 2002. Development of a three-dimensional semi-analytical elastic-plastic contact code. ASME Journal of Tribology 124 (4), 653–667.
Johnson, K.L., 1985. Contact Mechanics. Cambridge University Press, London, UK.
Kabo, E., Ekberg, A., 2002. Fatigue initiation in railway wheels – a numerical study of the influence of defects. Wear 253, 26–34.
Kabo, E., Ekberg, A., 2005. Material defects in rolling contact fatigue of railway wheels – the influence of defect size. Wear 258, 1194–1200.
Kuo, C.-H., 2007. Stress disturbances caused by the inhomogeneity in an elastic half-plane subjected to contact loading. International Journal of Solids and Structures 44, 860–873.
Kuo, C.-H., 2008. Contact stress analysis of an elastic half-plane containing multiple inclusions. International Journal of Solids and Structures 45, 4562–4573.
Liu, S., Wang, Q., 2005. Elastic fields due to eigenstrains in a half-space. ASME Journal of Applied Mechanics 72, 871–878.
Liu, S., Chen, W.W., Hua, D., Wang, Q., 2007. Tribological modeling: application of fast Fourier transform. Tribology International 40, 1284–1293.
Love, A.E.H., 1927. A Treatise on the Mathematical Theory of Elasticity, fourth ed. Cambridge University Press, Cambridge, UK.
MacMillan, W.D., 1930. Theory of the Potential. McGraw-Hill, New York.
Miller, G.R., Keer, L.M., 1993. Interaction between a rigid indenter and a near-surface void or inclusion. ASME Journal of Applied Mechanics 50, 615–620.
Mindlin, R.D., Cheng, D.H., 1950. Thermoelastic stress in the semi-infinite solid. Journal of Applied Physics 21, 931–933.
Moschovidis, Z.A., Mura, T., 1975. Two-ellipsoidal inhomogeneities by the equivalent inclusion method. ASME Journal of Applied Mechanics 42, 847–852.
Mura, T., 1987. Micromechanics of Defects in Solids, second ed. Martinus Nijhoff, Dordrecht.
Mura, T., 1988. Inclusion problem. ASME Journal of Applied Mechanics Review 41, 15–20.
Mura, T., Furuhashi, R., 1984. The elastic inclusions with a sliding interface. ASME Journal of Applied Mechanics 51, 308–310.
Nélias, D., Dumont, M.-L., Champiot, F., Vincent, A., Girodin, D., Fougères, R., Flamand, L., 1999. Role of inclusions, surface roughness and operating conditions on rolling contact fatigue. ASME Journal of Tribology 121 (2), 240–251.
Nélias, D., Boucly, V., Brunet, M., 2006. Elastic-plastic contact between rough surfaces: proposal for a wear or running-in model. ASME Journal of Tribology 128 (2), 236–244.
Nélias, D., Antaluca, E., Boucly, V., Cretu, S., 2007. A 3D semi-analytical model for elastic-plastic sliding contacts. ASME Journal of Tribology 129 (4), 761–771.
Nélias, D., Antaluca, E., Boucly, V., 2007. Rolling of an elastic ellipsoid upon an elastic-plastic flat. ASME Journal of Tribology 129 (4), 791–800.
Sainsot, P., Jacq, C., Nélias, D., 2002. A numerical model for elastoplastic rough contact. Computer Modeling in Engineering and Sciences 3 (4), 497–506.
Seo, T., Mura, T., 1970. The elastic field in half space due to ellipsoidal inclusions with uniform dilatational eigenstrains. ASME Journal of Applied Mechanics 46, 568–572.
Voskamp, A.P., 1985. Material response to rolling contact loading. ASME Journal of Tribology 107, 359–366.
Walpole, L.J., 1967. The elastic field of an inclusion in an anisotropic medium. In: Proceedings of the Royal Society of London, A300, pp. 270–288.
Wang, F., Block, J., Chen, W.W., Martini, A., Keer, L.M., Wang, Q., 2009. A multi-scale model for the simulation and analysis of elasto-plastic contact of real machined surfaces. ASME Journal of Tribology 131, 021409-1–021409-6.
Willis, J.R., 1964. Anisotropic elastic inclusion problems. The Quarterly Journal of Mechanics and Applied Mathematics 17 (2), 157–174.
Zhou, K., Chen, W.W., Keer, L.M., Wang, Q.J., 2009. A fast method for solving three-dimensional arbitrarily shaped inclusions in a half space. Computer Methods in Applied Mechanics and Engineering 198 (9–12), 885–892.